International Journal of Engineering Trends and Technology
ISSN: 2231-5381/ https://doi.org/10.14445/22315381/IJETT-V74I6P128

Volume 74 Issue 6, 421-439 June 2026

Original Article

Metamaterial Inspired Open Ended Coupled Line Bandpass Filter using Twin Split Ring Resonators for X-Band RADAR and Satellite Communication

Gauravkumar R. Asari[1], Priti J. Muliya[2], Rina N. Bhatt[3], Ami B. Gandhi[4]

[1,3]*Department of Electronics and Communication Engineering, Vishwakarma Government Engineering College, Chandkheda, Ahmedabad, Gujarat, India.*
[2,4]*Department of Electronics and Communication Engineering, L.D. College of Engineering, Ahmedabad, Gujarat, India.*

[1]*Corresponding Author : grsasari@vgecg.ac.in*

Received: 07 February 2026 Revised: 07 April 2026 Accepted: 20 April 2026 Published: 27 June 2026

Abstract *- The research paper shows the development and optimization together with performance testing of a 9.7 GHz Bandpass Filter (BPF) which takes its design elements from metamaterials through the application of open-ended coupled lines that work with twin Split-Ring Resonators (SRRs). The research first conducts a complete structural and electromagnetic investigation of the SRR to study how different ring gap, ring width, and inter-ring distance dimensions affect the resonant behavior of the structure. The Nicolson Ross Weir (NRW) method uses full-wave S-parameter simulations to extract the effective permittivity and permeability of the resonator, which shows negative permittivity and magnetic resonance near the operating frequency. The filter design uses an RT/Duroid 4003 substrate (εr = 3.55, h = 0.85 mm) and places twin SRRs at specific locations, which boost electromagnetic coupling within the coupled-line section. The research demonstrates that SRR loading enhances electric-field confinement through its ability to create new paths for capacitive inductive interaction, while it also improves near-field coupling. The filter shows 1.26 GHz bandwidth improvement together with 0.34 dB insertion loss reduction and 37.91 dB out-of-band rejection performance when compared to the filter design, which does not include SRRs. The inclusion of SRRs also sharpens selectivity by generating transmission zeros near the passband edges. The research results demonstrate better performance than existing studies in size, passband attenuation, reflection loss, bandwidth, rejection, and selectivity metrics. The SRR-loaded BPF achieves compact design with effective out-of-band suppression and minimal loss, which makes it suitable for RADAR front ends, satellite transceivers, and broadband microwave communication systems.*

Keywords *- Bandpass Filter, Split Ring Resonator, S Parameters, HFSS.*

1. Introduction

Bandpass Filters (BPFs) are indispensable components in microwave and high-frequency front-end systems because they define the usable spectrum, suppress unwanted harmonics and adjacent-channel interference, and directly affect receiver sensitivity and transmitter spectral purity. In X-band RADAR and satellite communication systems, the filter must simultaneously provide low insertion loss, adequate bandwidth, sharp selectivity, compact size, and strong out-of-band rejection.

These requirements become more demanding in modern platforms where the front-end must remain lightweight, planar, low-cost, and compatible with printed circuit integration. Conventional filter topologies often satisfy only a subset of these requirements, and therefore, the development of compact high-performance BPFs for X-band operation continues to be an active research problem [1]. Traditional lumped-element and planar microstrip filters are widely used because of their simple synthesis and fabrication convenience; however, their performance degrades as frequency increases toward the X-band region. Lumped filters suffer from parasitic inductance, parasitic capacitance, reduced quality factor, and self-resonance of practical components, which limit their usefulness in high-frequency RADAR and satellite front ends.

Cavity resonator filters can achieve excellent quality factor and low insertion loss, but their large volume, high weight, precision machining requirements, and limited suitability for planar integration make them less attractive for compact and low-profile microwave modules. Likewise, SAW and BAW filters are highly attractive in lower-frequency wireless systems, yet they generally exhibit constraints in bandwidth, power handling, and manufacturability for wideband X-band applications. Plasmonic and spoof surface plasmon-based filters provide

strong field confinement and wideband behavior, but they typically require intricate geometries, specialized transitions, and careful fabrication, which complicates their practical integration into conventional microwave subsystems. The literature survey in the manuscript already reflects these limitations across lumped, cavity, SAW/BAW, plasmonic, and conventional planar resonator filters.

Among planar microwave filters, coupled-line structures remain attractive because they are compact, easy to implement, and compatible with standard PCB fabrication. In particular, open-ended coupled-line filters can provide useful passband formation through even- and odd-mode coupling while maintaining a simple planar architecture. However, a conventional coupled-line filter still faces limitations in bandwidth control, near-passband selectivity, and suppression of undesired frequencies unless additional resonating elements or transmission-zero-generating mechanisms are introduced. This has motivated the use of metamaterial-inspired resonators as auxiliary loading structures for improving filter performance without excessively increasing size.

SRRs have emerged as powerful metamaterial-inspired elements because of their compact LC-type resonance, strong electric and magnetic field confinement, and ability to alter the effective electromagnetic response of planar circuits. Near resonance, SRRs can exhibit negative effective constitutive behavior and can introduce additional coupling paths that are not available in conventional resonator configurations. For microwave filters, this enables sharper selectivity, improved stopband attenuation, and miniaturization. Several SRR- and CSRR-based filters reported in the literature demonstrate the usefulness of metamaterial loading for improving bandwidth or rejection.

However, a close examination of prior work reveals that many of these filters are centered at lower microwave frequencies, exhibit narrow fractional bandwidth, rely on single resonator loading, or provide only moderate control over transmission zeros and out-of-band rejection. Even in the available X-band SRR-based filters, the passband is often narrow, the insertion loss is relatively high, or the structure does not exploit strong interaction between the resonator and the host transmission-line topology [1, 2]. The inherent LC characteristics of the system allow engineers to tune its resonant behavior by changing its physical design because these characteristics originate from the combination of ring inductance and capacitive gaps.

The recent metamaterial-loaded microwave circuit improvements show that SRRs can boost coupling efficiency, create transmission zeros, and increase microstrip filter bandwidths. The existing studies mostly depend on designs that operate within narrow frequency ranges or low-frequency limits, whereas they use SRRs in superficial ways without doing extensive research on all three parametric, electromagnetic, and material characteristics. To achieve optimal performance resulting from SRR geometry design, researchers need to study ring spacing and ring width and gap variation because they affect performance in systems that use coupled-line filters to control their passband characteristics through both even- and odd-mode interactions [3].

The problem addressed in this paper is therefore defined to realize a compact X-band bandpass filter for RADAR and satellite communication that overcomes the bandwidth and selectivity limitations of conventional open-ended coupled-line structures without sacrificing low insertion loss and manufacturability. To solve this problem, this work introduces a metamaterial-inspired BPF in which twin SRRs are strategically integrated into an open-ended coupled-line topology fabricated on RT/Duroid 4003 substrate.

The SRRs are not merely added as decorative resonators; instead, their geometry is first analyzed through parametric variation of ring gap, ring width, inter-ring Spacing, and substrate effect, and their effective electromagnetic behavior is verified through NRW parameter retrieval. The optimized resonators are then embedded in the coupled-line section to introduce additional inductive-capacitive coupling paths, strengthen field localization, and create a more selective passband response.

The novelty of the proposed work lies in four aspects. First, it combines an open-ended coupled-line BPF with twin SRR loading specifically for X-band operation, which is less explored than lower-frequency SRR filter designs. Second, the work connects unit-cell metamaterial analysis and circuit-level filter design in a single framework by performing both SRR parametric optimization and NRW-based effective parameter extraction before filter integration.

Third, the twin SRR arrangement creates enhanced near-field coupling and additional resonant interaction, leading to measurable improvement in filter characteristics compared with the unloaded filter. Fourth, the proposed filter achieves a favorable combination of compact size, low insertion loss, wider bandwidth, and improved out-of-band rejection, which compares well with the representative filters summarized in the manuscript. In particular, the inclusion of twin SRRs increases the bandwidth from 870 MHz to 1.26 GHz while improving out-of-band rejection from 25.46 dB and 14.10 dB to 37.91 dB and 21.08 dB, respectively, with insertion loss remaining very low.

Compared with existing research findings summarized in the literature review and comparative table, the proposed design distinguishes itself by targeting a practically relevant X-band frequency of 9.7 GHz using a compact planar configuration of approximately 16 × 10 mm^2, while still maintaining competitive insertion loss and fractional

bandwidth. Earlier cavity-based solutions offer excellent quality factor but at the cost of bulky three-dimensional structures, whereas several reported SRR/CSRR planar filters operate at lower frequencies or provide narrower fractional bandwidths. The present work, therefore, fills an important gap between compact planar manufacturability and enhanced electromagnetic performance for X-band front-end integration.

The remainder of this paper is organized as follows. First, a critical review of conventional and metamaterial-based filters is presented to establish the motivation for the proposed design. Next, the structural and electromagnetic analysis of the SRR is discussed, followed by effective parameter extraction using the NRW method. Thereafter, the open-ended coupled-line filter is analyzed using even- and odd-mode theory, and the integration of twin SRRs is introduced. Finally, the simulated filter performance is discussed and compared with reported literature to demonstrate the suitability of the proposed design for X-band RADAR and satellite communication systems.

2. Critical Review of Conventional and Metamaterial-Based Filters

2.1. Limitations of Lumped-Element Filters for X-Band RADAR Applications

In [4], a compact tri-band BPF runs at 0.8 GHz, 1.8 GHz, and 2.6 GHz and uses surface-mount components on a Rogers 4003C substrate with a thickness of 0.51 mm and a 15 mm × 20 mm area. From three Low-Pass Filter (LPF) portions, a bandpass filter is designed. Resonators with shunt topologies provide transmission zeros between passbands to improve isolation and reduce interference. For all three frequency bands, the reflection loss is about 15 dB, whereas the insertion loss is 1.1, 1.4, and 1.2 dB at 0.8, 1.8, and 2.6 GHz, respectively. The system has 290 MHz bandwidth at 0.8 GHz, 1.8 GHz, and 1 GHz at 2.6 GHz.

In [5], the researchers developed a filter that does not reflect signals. Traditional filters reflect signals, but the suggested structure absorbs them to identify stopband energy. Besides symmetrically placed shunt inductors and series capacitors, LPFs can have reactive elements added for tuning flexibility. By cascading filter sections for specified lower and upper pole frequencies, the BPF is achieved. Design uses even–odd mode analysis, which necessitates testing both ports with two approaches.

Superimposing the even- and odd-mode solutions yields the symmetric two-port network's response. The LPF has a peak stopband rejection of 53 dB, and the BPF has 43 dB. In their operational passband, the filters have 25 dB return loss. The LPF has a maximum attenuation point at 325 MHz, and the BPF has two cutoff frequencies at 110 and 310 MHz, creating a 200 MHz bandwidth. Studies reported in [6, 7] compact high-performance filters are being developed for mm-wave 5G small cell networks. An LPF and two BPFs target the 28 GHz and 39 GHz frequency bands, respectively. All filters are made using the Semi-Additive Process (SAP), which ensures accurate dimensional measurements throughout production runs. To work, the LPF needs 4.23 × 1.42 mm², the interdigital BPF 3.06 × 2.26 mm², and the hairpin BPF 3.85 × 1.22 mm². LPF designs run at 29.5 GHz using normalized prototype g-values to extract inductance and capacitance values for guided wavelength microstrip dimension calculation.

The 28 GHz interdigital BPF uses parallel quarter-wavelength short-circuited resonators with adjustable Spacing to vary coupling strength and bandwidth. The system creates an abrupt roll-off and continuous in-band ripple with a Chebyshev response. To reduce circuit size, designers constructed U-shaped half-wavelength resonators employing Chebyshev polynomials for the 39 GHz hairpin BPF. Insertion loss values for the LPF, interdigital BPF, and hairpin BPF are 2.0, 2.6, and 1.4 dB, respectively, whereas reflection loss values are 1517 dB. The interdigital BPF has 18% fractional bandwidth, and the hairpin BPF 16%.

X-band RADAR and satellite communication systems cannot use lumped-element filters with discrete inductors and capacitors due to physical restrictions. At 8-12 GHz, discrete components provide parasitic inductances and capacitances that regulate circuit behavior, reducing filter performance. Due to their self-resonant frequencies below X-band, practical inductors and capacitors have increased insertion loss, lower selectivity, and unpredictable frequency response patterns. The filters fail power-handling criteria for RADAR transmit chains. Lump-element filters cannot meet the sharp roll-off, low loss, and electromagnetic stability criteria of high-frequency RADAR and satellite front-end systems.

2.2. Limitations of Cavity Resonator Filters in Compact RADAR Front-Ends

In [8], a TE_{011} mode resonator-based adjustable Ka-band cavity BPF with a mode-splitter construction and dual coupling mechanisms is presented. TE_{011} is chosen because it has reduced insertion loss and is less susceptible to degenerate TM modes. To prevent mode degeneracy, the cavity end walls use a metal-ring mode splitter with a peripheral channel and central bore. The technology couples energy between resonators using short and long irises.

A sliding contact mechanism provides electrical continuity during frequency tuning, and a moveable tuning plate on plungers alters the effective cavity length. To improve stability and reduce dimensional sensitivity, the system uses extended irises to connect all coupling paths, creating a pseudo low-pass filter. The filter design uses a pseudo-High-Pass Filter (HPF) with a wide iris for sequential coupling and a smaller one for cross-coupling. From 20 GHz to 500 MHz, the

filter's center frequency can be modified, and its bandwidth can be tuned between 40 and 160 MHz. The system has 0.3 dB insertion loss and 17 dB return loss. The filter, built using typical precision machining methods, measures 110 × 22 × 20 mm^3.

In [9], the performance issues of typical TE_{011} and TE_{1N} dual-mode filters are solved by a Ka-band cavity filter. The design employs the TE_{221} mode because its unloaded quality factor is 50% higher than that of the TE_{011}. TE_{221} modes at orthogonal angles are coupled intra-cavity to create dual-mode functionality. Inter-cavity coupling uses end-wall and side-wall irises to connect adjacent hollow walls. A four-pole filter has four resonator cavities connected by radial and angular irises. The filter operates at 19.9 GHz, with 0.4 dB insertion loss, 17 dB return loss, 44 MHz bandwidth, and 140 × 145 × 25 mm^3 physical space.

The study reported in [10] has developed two innovative cavity filter designs, inline and vertical, to improve space efficiency and system performance. Engineers place end-launched ports in straight lines in the inline configuration, while angular irises improve inter-cavity coupling and prevent undesired signals. The vertical layout uses side-launched ports to place all connections on one side of the structure, reducing space. A 2A1R iris construction improves signal rejection outside its frequency range. The inline filter is 145 × 35 × 25 mm^3, whereas the vertical pattern is smaller at 35 × 35 × 25 mm^3.

In [11], A stepped circular waveguide dual-mode filter design for Ku-band applications increases the capabilities of conventional filters. Cavity step designs reduce spurious signals and expand design possibilities. Iris coupling transfers energy across cavities, and tuning screws near the electric field peak points allow designers to maintain equal phase between overlapping modes and set operational frequencies. The filter operates at 10.73 GHz, with 0.5 dB insertion loss, 17 dB return loss, 54 MHz bandwidth, and 208 × 30 × 30 mm^3 size.

In [12], a high-Q Hybrid Resonator (HR)-based BPF is used to produce a compact diplexer with good selectivity and small dimensions. A hybrid resonator uses microstrip line and short-circuited coaxial line technology to create a high-Q element that improves system quality. Mixed electromagnetic coupling creates fine selectivity and a wider bandwidth by combining electric and magnetic coupling. RT/Duroid 5880 substrates with 0.508 mm thickness and 2.2 relative permittivity are used to make the filters, which are enclosed in metal to prevent external influence.

The diplexer, with a 27.1 × 1.8 × 10 mm^3 volume, achieves 1.5 dB insertion loss and 40 dB channel isolation, with passbands of 80 MHz and 102 MHz at 2.4 GHz and 2.7 GHz center frequencies. [13] improves the hybrid resonator system from [12] by adding shape deformation algorithms to improve filter performance. Because the deformation approach uses control points and displacement vectors to change three-dimensional shapes, the resonator structure and coupling mechanisms remain the same. This approach lets resonators and waveguides bend, twist, and compress while better separating fundamental and higher-order modes. Through cavity geometry optimization, optimal cavity designs produce wider spurious-free regions and better quality factors. The filter operates at 14.25 GHz with 0.5 dB insertion loss, 17 dB return loss, 54 MHz bandwidth, and 18.77 × 18.77 × 12.72 mm^3 dimensions.

Cavity resonator filters' high-quality factor and low insertion loss enable microwave applications. Its restrictions limit its application in X-band RADAR systems and satellite platforms. X-band resonant cavities are big and heavy, making them difficult for airborne, spaceborne, and phased-array RADAR systems to meet size and weight requirements. Because cavity filters require precision machining, tuning screws, and mechanical alignment, manufacturing is more complicated and expensive.

Mechanical tuning systems suffer from heat drift and vibration sensitivity, which reduces their durability in harsh situations. Cavity filters are difficult to integrate with planar microwave circuits and tiny RF front-end modules, limiting their application in high-integration RADAR systems and satellite transceivers.

2.3. Performance Limitations of SAW and BAW Filters at X-Band

In [14], the filter design starts with a low-pass Bessel prototype, an all-pole structure optimized for a flat group delay response. The technology converts a low-pass response to a BPF using frequency transformation. Instead of LC resonators, the Bessel-type BPF uses SAW or BAW resonators. The practical implementation employs a Cu-grating on a 15°YX-cut $LiNbO_3$ substrate, chosen for its strong electromechanical coupling in SH SAW modes. From the 980 megahertz midpoint, group-delay changes of 3 nanoseconds were observed over 15 megahertz.

The filter has a 4 × 2 mm^2 size, 5.3 dB insertion loss, 15 dB return loss, and 30 MHz bandwidth. A hybrid RF filter design method using high-Q SAW resonators and lumped-element impedance inverters is described in [15]. The technology eliminates the biggest drawbacks of ladder and lattice acoustic filters: restricted fractional bandwidth and group-delay fluctuations.

The design heavily uses Acoustic Wave Lumped Resonators (AWLRs) connected by impedance inverters with discrete inductors and capacitors. Impedance inverters are crucial for bandwidth management and group-delay response flattening. Two AWLRs connected through three impedance inverters form the two-pole bandpass filter, which was built

on a Rogers RO4003 substrate with a thickness of 1.52 mm and a dielectric constant of 3.55. This small 15 × 7 mm² filter runs at 418 MHz center frequency, with insertion loss of 1.5 dB, return loss of 17 dB, and 450 MHz bandwidth.

In [16], the BPF design for 5G applications using SAW and BAW resonators made of AlN is investigated. The study examines two main resonator designs, which include Thin-Film Bulk Acoustic Resonators (TFBARs) and Solidly Mounted Resonators (SMRs). TFBARs employ an air cavity beneath the resonator to confine acoustic energy, while SMRs use Bragg reflectors with many layers of varying impedances to keep it from reaching the substrate. SMRs are ideal for 5G applications due to their mechanical strength and severe temperature performance.

The study compares ladder-type, lattice-type, stacked crystal, and coupled-resonator acoustic filters. Ladder-type filters use series and shunt resonators at distinct frequency points to provide a sharp roll-off near the passband but weak signal rejection beyond it.

Lattice filters use resonators to improve stopband performance but diminish passband signal selection. Stacked crystal filters use multilayer piezoelectric and metallic sheets for compactness and low insertion loss. Coupled-resonator filters reduce resonator effects and double the bandwidth of stacked crystal filters by coupling through a dedicated layer. Acoustic filters with typical performance tests exhibit insertion loss of 3 dB, return loss of 18 dB, and bandwidth of 5% to 10% of center frequency in a compact 3 × 5 mm² area.

The study in [17] provides detailed information regarding SAW filter technologies that focus on new material developments, improved manufacturing procedures, and design strategies for 5G networks and high-frequency RF systems. Interdigital Transducers (IDTs) and reflectors make conventional SAW filters efficient in low-frequency situations with narrowband signal processing. Multiple resonators and clamping capacitors give dual-mode SAW filters multimodal capacity for sophisticated filtering. The industry generally uses $LiNbO_3$ and $LiTaO_3$ substrates for their good piezoelectric coupling, whereas aluminum and Ti/Cu multilayer electrodes are used for their reduced resistive losses.

In [18], BAW resonator designs with improved SiO_2/Ta_2O_5 Bragg reflectors are investigated for 5G technology. SMR-based systems outperform FBARs for frequencies above 3 GHz due to their better structural strength, electromechanical coupling, and multi-frequency operation. The resonator construction uses a Lithium Niobate (LN) thin film between aluminum electrodes, while the Bragg reflector stack switches between low-impedance SiO_2 and high-impedance Ta_2O_5 layers. Using a 5 × 5 mm² area, the 3.5 GHz ladder-type BPF achieved 1.9 dB insertion loss, 19 dB return loss, and 245 MHz bandwidth. The study in [19] shows AlScN-based BAW resonators operating at 5G frequencies approaching 3.5 GHz. Resonators with 28% scandium doping have greater electromechanical coupling than AlN materials. Cross-sectional bulk acoustic wave (XBAW) resonators reduce energy loss and improve acoustic confinement. The filter delivers 1.2 dB insertion loss, 18 dB return loss, 216 MHz bandwidth, and approximately 15% electromechanical coupling coefficient in a compact 0.8 × 0.8 mm² design. In [20], a wideband acoustic transversal filter designed for 5G applications is shown in the research.

The transversal architecture connects numerous acoustic resonators via parallel branches, creating independent signal channels. Because transmission zero points and bandwidth parameters are not impacted by electroacoustic coupling coefficients, the system allows filter construction with varied filter responses. The technique lets designers develop wideband systems with fewer resonators than before. Resonator frequency optimization, coupling strength, and impedance level changes give the filter 2 dB insertion loss at 3.75 GHz center frequency, 16 dB return loss, and 910 MHz wide passband. A 13% electroacoustic coupling coefficient is observed, using a filter dimension of 0.5 × 0.5 mm².

The small size and strong frequency stability at low frequencies make SAW and BAW filters popular in commercial wireless systems. Their use for X-band RADAR and satellite communication is limited. Because X-band electrode spacing exceeds manufacturing capacities, SAW filters operating at high frequencies suffer from considerable performance loss and unreliability due to lithographic restrictions.

BAW filters can operate at frequencies higher than SAW devices, but their narrowband design limits X-band fractional bandwidth. The SAW and BAW filters have power handling, thermal management, and nonlinear effects that cause RADAR transmit-receive module issues. The system is least efficient since it needs wideband functionality, high power, and good out-of-band blocking.

2.4. Plasmonic Filters and their Suitability for RADAR Applications

In [21], BPFs using Substrate-Integrated Plasmonic Waveguides (SIPWs) between 7.5 GHz and 13.0 GHz are studied. The suggested filter uses copper metallization on a 0.5-mm Rogers 5880 substrate with a relative permittivity of 2.2. Etching regular patterns onto the upper and bottom metal layers of a Substrate Integrated Waveguide (SIW) system creates the SIPW structure and Spoof Surface Plasmon Polariton (SSPP) phenomena. The topology is microstrip-SIW-SIPW-SIW-microstrip. A tapered microstrip-to-SIW transition allows the system to seamlessly switch between quasi-TEM and quasi-TE operational modes for broadband capabilities. A graded slot-length profile allows momentum

adaptation and impedance matching from the quasi-TE mode to the SSPP mode during the SIW-SIPW transition. The filter has a center frequency of 10.25 GHz, insertion loss of 1.5 dB, return loss of 10 dB, and over 40% fractional bandwidth in a 36 × 18 mm² footprint.

In [22], the researchers created a simple but efficient X-band bandpass filter from 7.3 to 10.1 GHz using SIPW and SSPP. Fishbone- and hourglass-shaped grooves improve electromagnetic field management and signal coupling, allowing mushrooming-faced slot antennas to broadcast military messages. The filter is made of 0.5-millimeter FR-4 with a dielectric constant of 4.3. A fishbone-shaped transition area connects microstrip lines to SSPP/SIPW transmission paths, a filtering area with hourglass-shaped grooves enables SSPP-based bandpass operations, and the system's main transmission path is the SIPW section. The filter center frequency is 8.7 GHz. It has about 2 dB insertion loss. The return loss is about 10 dB. The system offers 32% fractional bandwidth. The device occupies a 34.4 × 12.2 mm² area.

The research described in [23] uses SSPP transmission lines with Rogers 5880 substrate material with 1.5 mm thickness and 2.2 dielectric constant. A unique H-shaped SSPP unit cell is used in the filter, which operates at microwave frequencies between 1.2 GHz and 6.0 GHz. The system has four components: a Coplanar Waveguide (CPW) feed for 50-Ω impedance matching, a transition section for mode conversion between CPW and SSPP, a periodic SSPP transmission line for plasmonic wave movement, and an LC resonator for bandpass filtering. The filter has a 2 dB insertion loss, 10 dB return loss, and 41% fractional bandwidth in a 26 × 4 mm² size.

In [24], researchers produced ultra-strong electromagnetic field confinement with reduced propagation loss using Planar I-shaped Plasmonic Waveguides (PIPWs). The I-shaped groove has lateral extensions at both ends to increase capacitive loading and electric field spatial control. The filter structure has a CPW feeding portion, a transition zone for quasi-TEM to SSPP mode conversion, and an SSPP transmission-line section. The filter operates from 1 to 5.2 GHz on an F4B substrate with a relative permittivity of 2.65 and a thickness of 0.5 mm. The insertion loss is around 1.5 dB, the return loss is around 12 dB, and the fractional bandwidth is at 42%, despite the larger size of 104 × 35 mm².

Field confinement and wideband performance are achieved by plasmonic microwave filters, but they fail to meet compact X-band RADAR and satellite communication system requirements. Surface current density increases and microwave energy is lost through precise metal groove patterns in SSPP and SIPW structures, causing microwave frequency propagation. Because plasmonic transmission line components extend farther, insertion loss rises. Fishbone, hourglass, and I-shaped groove designs demand precise manufacturing methods and dimension measurement to create complicated goods. Traditional planar RF front-end systems cannot combine plasmonic waveguide filters because they require specific interface components and nonstandard dimensions. Due to restrictions in plasmonic filter applications for tiny X-band RADAR and satellite communication front-end modules, new planar metamaterial-inspired filter designs are developed.

2.5. Constraints of Conventional Planar Resonator Filters

In [25], the research addresses parallel-coupled dual-mode resonator BPF design development. Dual-mode resonators provide two non-degenerate resonant modes, allowing higher-order filtering responses with fewer physical resonators. The dual-mode resonator circuit has two coupled resonators connected by an admittance inverter and susceptance elements. The design creates a four-pole microstrip bandpass filter on a RO4003C substrate with a relative permittivity of 3.36 and a thickness of 0.5 mm to obtain a 1 GHz center frequency.

Due to fabrication tolerances, dielectric constant change, and coupling imperfections, the center frequency has dropped from 1.0 GHz to 0.968 GHz, according to experimental observations. The filter exhibits significant stopband rejection, with initial spurious answers at $2.88f_0$ and $3.12f_0$ instead of $2f_0$, indicating improved harmonic suppression. Measured insertion loss is 2.5 dB, return loss is 15 dB, bandwidth is 98.6 MHz, and physical size is 30 × 20 mm².

The study presented in [26] investigates Ultra-Wideband (UWB) Bandpass filters with tapered transmission-line resonators for 3.1 GHz to 10.6 GHz operation. Compact tapered resonators offer greater stopband performance and a wider operational range than traditional transmission-line resonators. Exponential Tapered Transmission Lines (ETTLs) vary impedance through their resonator length, while Linear Tapered Transmission Lines (LTTLs) change impedance linearly.

UWB BPF uses tapered resonators instead of standard elements with different taper ratios to change bandwidth and stopband performance. Higher taper ratios extend bandwidth and reduce out-of-band interference. Four short-circuited tapered stubs connect through uniform transmission-line sections less than half their length to produce the filter structure.

Rogers RT5880 substrates with 2.2 relative permittivity and 0.78 mm thickness were used to build the filter. The filter operates at 6.8 GHz with a 2.5 dB insertion loss and 15 dB return loss, fitting within a 30 × 20 mm² space.

In [27], the multilayer ultra-broadband bandpass filter uses high impedance slotline resonators to reduce radiation loss and improve stopband performance. The revised

resonator design replaces the single short-circuited high-impedance slotline segment with two shunt-connected folded low-impedance slotline sections to reduce radiation and improve microstrip circuit impedance matching. The research team constructed an ultra-wideband microstrip-to-microstrip vertical transition to connect slotline resonators to multilayer filter systems. The transition design's base model combines coupled microstrip and slotline resonators for broadband operation. The seven-pole Chebyshev equiripple bandpass filter uses a Rogers 4003C substrate with 2.2 relative permittivity and 0.81 mm thickness. The filter has a 21 × 10 mm² size and operates at 2 GHz with 1.3 dB insertion loss and 13 dB return loss.

The design presented in [28] builds a microstrip bandpass filter with Bluetooth and WLAN features using a polygonal open-loop resonator for size efficiency and passband operation. The suggested filter uses two polygonal open-loop resonators with 11 different-length segments to vary electrical length without adding space.

This approach lets open-loop resonators operate at smaller sizes with selective performance and low insertion loss. At 2.4 GHz, the filter operates on a Rogers RO3010 substrate with a dielectric constant of 10.2 and a thickness of 1.5 mm. Measurements indicate a 230 MHz bandwidth, 1.2 dB insertion loss, and 25 dB return loss in an 8 × 16 mm² compact region.

The structural design of planar resonator-based filters, such as parallel-coupled line filters, dual-mode resonators, and tapered transmission-line resonators, for X-band RADAR and satellite communication systems is difficult. Since narrowband and ultra-wideband microwave filters have higher conductor and dielectric losses and insertion loss, they are inappropriate for X-band operation. Planar resonators produce undesirable harmonic responses that affect out-of-band performance, requiring further suppression measures such as defective ground structures or more resonators that complicate design and increase circuit dimensions. Traditional planar resonators cannot accomplish the needed X-band selectivity and out-of-band rejection in confined locations. Metamaterial-inspired planar filter structures improve electromagnetic control, smaller size, and X-band RADAR and satellite front-end performance; therefore, the study studies them.

2.6. Suitability of Electromagnetic Resonator-based Filters using SRR and CSRR

In [29], a 2.4 GHz Split-Ring Resonator (SRR) BPF design is shown. Ring length, width, gap, and inter-ring Spacing determine the resonant behavior of the SRR unit's two concentric rings, an outer and an inner. The filter's coupling strip controls energy transfer between the SRR and the feeding structure. To connect to external circuits, the filter uses a microstrip transmission line. The sequential arrangement of three SRR elements with optimal inter-element Spacing increases filtering performance. The filter utilizes a 25 × 19 mm² Rogers RT/Duroid 6010/6010LM substrate with a 10.2 relative permittivity and 1.9 mm thickness. The measured findings show 2.5 dB insertion loss, 16 dB return loss, and roughly 5% fractional bandwidth.

A parallel-coupled microstrip BPF with SRR and CSRR elements has been used to create a 1 GHz operating system [30]. Parallel-coupled microstrip lines form the system's passband. Engineers put two stepped-impedance stubs symmetrically to improve selectivity around the resonator point. The basic system design generates undesirable harmonics and fails to reject signals outside its stopband range. SRRs, CSRRs, and stepped-impedance stubs fix these problems and improve performance.

The system uses SRR and CSRR elements to provide low insertion loss and excellent stopband rejection between 1.22 GHz and 5 GHz. The filter uses FR-4 substrate material with a dielectric constant of 4.4, a thickness of 1.6 mm, and a space of 30 × 18 mm². It has an insertion loss of 1.1 dB, a return loss of around 16 dB, and a fractional bandwidth of 21%.

In [31], a narrowband X-band bandpass filter with two circular SRR rings is described. A microstrip feedline excites and matches the resonator's impedance. The filter response is adjusted by systematic change of SRR parameters such as ring gap, width, and Spacing. Increasing the ring gap or breadth raises the resonant frequency, while lowering them lowers it. After changing the inter-ring Spacing, the central frequency remains unchanged. The filter is constructed on Rogers RT/Duroid 5880 substrate, with a 2.2 relative permittivity, 0.5 mm thickness, and 25 × 22 mm² area. The observed center frequency is 9.0 GHz, with an insertion loss of 3.7 dB, a return loss of 15 dB, and a narrow fractional bandwidth of roughly 1%.

The research in [3] shows twin SRRs and CSRRs electromagnetically interacting to generate a dual-band bandpass filter. The first arrangement uses twin SRRs with weak coupling because their outward-facing gaps provide two passbands at 5.02 GHz and 8.92 GHz. When oriented to face each other, SRR gaps couple better, expanding the lower band range from 230 MHz to 320 MHz.

Because it generates a notch-filtering effect that eliminates undesirable signals throughout the passband, a CSRR improves twin SRR coupling. The filter creates more exact transitions and improves signal separation. The 16 x 24 mm² filter, built on Rogers RO4003 substrate with 3.55 dielectric constant and 0.85 mm thickness, exhibits 6.22 dB and 5.23 dB insertion losses in lower and upper bands, respectively, with 6% and 3% fractional bandwidths.

The research presented in [32] shows a circular split-ring resonator-based microstrip bandpass filter. The SRR, two

concentric rings with capacitive gaps, is the principal resonating element. Microstrip feedlines with 50 Ω impedance power the resonator. The capacitive gaps and inductive rings form an LC resonant circuit that sets the operation frequency. Rogers RT/Duroid 6010 substrate, with 11.4 relative permittivity and 1.9 mm thickness, is used to build a 25 × 25 mm² filter design. The experimental results show a 2.4 GHz center frequency, 1.3 dB insertion loss, 18.8 dB return loss, and 5% fractional bandwidth.

Research in [33] analyzes how substrate permittivity and thickness affect square-shaped double split-ring resonators' functioning. When substrate permittivity increases, resonator effective capacitance increases, decreasing resonant frequency and bandwidth. The bandwidth widens, and resonance rises as permittivity decreases. Small effective capacitance increases with substrate thickness decrease, resonance frequency, but improves electromagnetic coupling and fringing fields to increase bandwidth. Thinner substrates have better confinement and fewer losses but lower coupling strength.

In [34], a BPF system with parallel-coupled lines and two ground plane CSRRs is shown. The microstrip-linked lines allow signal flow and interaction, while the CSRRs add resonant routes for selectivity and bandwidth management. Parametric optimization of CSRR size and coupling gaps improves impedance matching and reduces insertion loss. The filter, which uses a 0.5-mm Rogers RT/Duroid 5880 substrate, operates at 3.6 GHz with an insertion loss of 1.6 dB, a return loss of 17 dB, and a fractional bandwidth of 5% in a 27 mm × 14 mm region.

The effect of adding SRRs to a microstrip structure is studied in [35] using an SRR-based band-stop filter. Attenuation and stopband are limited by a single SRR, although electromagnetic coupling and resonance strength increase with more SRRs. Three SRRs produce 19 dB attenuation, whereas six SRRs produce 30 dB rejection with an expanded stopband. Advanced connections between numerous SRRs increase energy absorption and stopband performance.

[36] present a multiband SRR BPF design for 2.4 GHz, 4.5 GHz, and 5.2 GHz. Three SRR unit cells with distinct resonance frequencies are used. An etched slot near the center of the microstrip transmission line improves frequency selectivity in the system's primary signal channel. The analysis demonstrates that SRR width improves return loss and length improves insertion loss. The filter, built on a 1.6 mm FR-4 substrate, occupies a 26 × 18 mm² space and exhibits insertion losses of 1.0 dB, 1.4 dB, and 2.1 dB across its three operational frequency bands.

In [37], SRR arrays connected to a microstrip line are used to build a cut-band filter. The study explores how SRR numbers, dimensions, and positioning patterns affect bandwidth and rejection. Through better coupling, additional SRRs improve rejection performance, while varied sizes prolong the stopband.

Multiple SRR rows improve electromagnetic interaction and rejection performance without adding filter design space. The balance between high rejection depth and passband performance is shown by excessive SRR stacking, which lowers transmission levels. Current SRR and CSRR small microwave filters have fundamental design problems that limit their use in X-band RADAR and satellite communication systems.

Most SRR-based filters in research operate at lower microwave frequencies or have limited fractional bandwidths, limiting their applicability in wideband X-band systems. In most applications, single or weakly coupled SRR designs generate challenges because of their low electromagnetic coupling, sluggish roll-off, and limited transmission zero management.

Cascaded SRRs improve stopband rejection but increase insertion loss, production variance, and circuit size. SRRs and standard microstrip feeding networks have little interaction, resulting in poor impedance matching and limited tuning possibilities.

The existing limitations show that highly coupled planar metamaterials are needed to achieve precise selectivity, minimal insertion loss, small dimensions, and strong out-of-band attenuation in the X-band range, which supports the planned open-ended coupled-line bandpass filter design with twin SRRs.

3. Structural Analysis of Split Ring Resonator

The SRR functions as a crucial element in metamaterials that facilitates the development of Left-Handed Materials. SRRs comprise two metallic rings that manifest as concentric circles or square configurations. The ring construction features a gap that generates capacitance between the two sections of the gap.

Figure 1 depicts the square-shaped SRR [38].Because the D gaps are created by the symmetrical gap arrangement, which inhibits field leakage, the electric field distribution remains uniform.

The energy radiation increases due to the fact that the gaps have a common orientation, resulting in more losses. Because they keep energy from leaving, the structure's opposing gaps serve to balance the system. By amplifying the system's magnetic field via the large magnetic flux they generate via induced currents, the two rings are able to keep moving in the same direction.

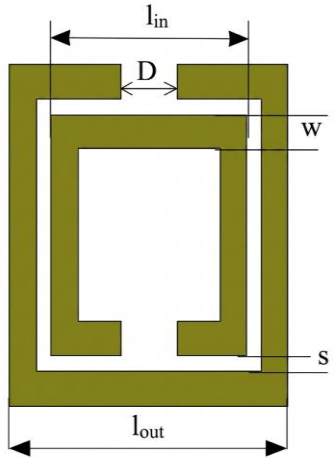

Fig. 1 Geometry of Square-Shaped SRR

With a reduced inter-ring distance S, SRRs are able to focus localized fields more effectively, making them metamaterial waveguides. As d increases, the electric field distribution becomes less concentrated and less efficient. The strength of magnetic coupling between rings is proportional to their distance from one another.

As the d-value drops, the rings exhibit higher mutual inductance due to the stronger resonance effects and deeper resonance patterns that result. As the ring width 'w' gets smaller, the electric field gets more concentrated, and its distribution pattern changes to try to keep it from spreading too far out in space. The control of the magnetic field is weaker with a larger ring because its inductance per unit length is lower, whereas the linking of magnetic flux is improved with a narrower ring.

3.1. Influence of Ring Parameters on Resonance Frequency

The SRR's inductive (L) and capacitive (C) characteristics essentially regulate its resonance frequency, f_0. The relationship is given by [38]

$$f_0 = \frac{1}{2\pi\sqrt{LC}} \tag{1}$$

where L is defined by the width and length of the rings, and C is formed by the specifications of the gap between the rings and the Spacing between them.

3.2. The Effect of the Ring Gap on the Capacitance

The gap (d) creates a capacitance C_{gap} defined by [38]

$$C_{\text{gap}} = \frac{\varepsilon_0 \varepsilon_r A}{D} \tag{2}$$

The relative permittivity of the dielectric material is denoted by ε_r, and 'A' stands for the capacitor's cross-sectional area. The resonance frequency f_0 rises as the capacitance falls with a larger gap. The opposite is true with a smaller gap: the resonance frequency f_0 drops as capacitance rises.

3.3. Ring Width's Effect on Inductance

The inductance L_m of the structure is influenced by the ring Width (W) [38]

$$L_m = \mu_0 (l_{\text{out}} + l_{\text{in}}) \frac{W}{S} \tag{3}$$

Narrower rings have a lower resonance frequency f_0 and a higher inductance, whereas wider rings have a higher resonance frequency f_0 and a lower inductance.

3.4. Influence of Ring Width on Inductance

The length of the Ring (l) influences the total inductance (L) [38].

$$L_m \propto l_{\text{out}} + l_{\text{in}} \tag{4}$$

Resonance frequency f_0 drops as inductance rises with increasing ring length. On the other hand, the resonance frequency f_0 increases due to a decrease in inductance caused by shorter rings.

Hence,

$$f_0 = \frac{1}{2\pi\sqrt{L_{\text{eq}} C_{\text{eq}}}} \tag{5}$$

where

$$L_{\text{eq}} = \mu_0 (l_{\text{out}} + l_{\text{in}}) \frac{W}{S}$$

$$C_{\text{eq}} = C_{\text{gap}} + C_m$$

4. Nicolson Ross Weir (NRW) Method for Parametric Extraction of the Split Ring Resonator

The NRW [39] technique calculates the complex permittivity $\varepsilon = \varepsilon_r \varepsilon_0 = (\varepsilon_r' - j\varepsilon_r'')\varepsilon_0$ and complex permeability $\mu = \mu_r \mu_0 = (\mu_r' - j\mu_r'')\mu_0$ of a material through the analysis of S-parameters derived from reflection and transmission measurements.

4.1. Correlation between S-Parameters and Reflection/Transmission Coefficients

$$S_{11} = \frac{(1-P^2)\Gamma}{1-P^2\Gamma^2} \tag{6}$$

$$S_{21} = \frac{(1-\Gamma^2)P}{1-P^2\Gamma^2} \tag{7}$$

where

$P = e^{-jk_2 d}$ is the propagation factor within the material.
Γ is the interfacial reflection coefficient expressed as

$$\Gamma = \frac{Z-Z_0}{Z+Z_0} \quad (8)$$

Z represents the wave impedance of the material, while Z_0 denotes the wave impedance of free space.

4.2. Extraction of Γ and P

Establishing the intermediate quantities

$$V_1 = S_{21} + S_{11} \quad (9)$$

$$V_2 = S_{21} - S_{11} \quad (10)$$

Solving for Γ

$$\Gamma = X + s_1\sqrt{X^2 - 1} \quad (11)$$

where

$$X = \frac{1-V_1V_2}{V_1-V_2} = \frac{1-S_{21}^2+S_{11}^2}{2S_{11}}$$

Solving for P

$$P = \frac{V_1-\Gamma}{1-V_1\Gamma} \quad (12)$$

Evaluating the propagation constant within the material, k_z

$$k_z = \frac{n-\phi}{2\pi}\frac{1}{d/\lambda_0} + j\frac{\ln|P|}{2\pi}\frac{1}{d/\lambda_0} \quad (13)$$

d represents the thickness of the sample, λ_0 denotes the free-space wavelength, and n signifies the branch number.

4.3. Extraction of εr and μr

$$\varepsilon_r = k_z F \quad (14)$$

$$\mu_r = \frac{k_z}{F} \quad (15)$$

where k_z is the wavenumber within the material, and F is defined as

$$F = \frac{1-\Gamma}{1+\Gamma} \quad (16)$$

5. Proposed Metamaterial Resonator

The suggested unit cell has the dimensions listed in Table 1 and shown in Figure 2. An RT/Duroid 4003 substrate with a relative permittivity of 3.55 and a thickness of 0.85 mm is utilized by the resonator, which runs at a center frequency of 9.7 GHz. By plugging the values into the appropriate equations, we get an inductance of 4.90 nH and a capacitance of 54.92 pF. The dimensions of the resonator have been further finely tuned and are mentioned in Table 2.

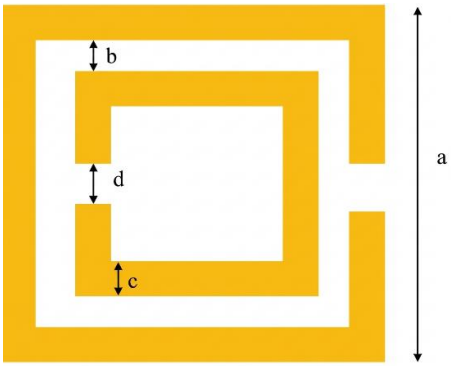

Fig. 2 Proposed SRR

Table 1. Dimensions of the SRR

Parameter	Dimensions
Length of Ring, a	5.0 mm
Inter-ring Spacing, b	0.3 mm
Width of Ring, c	0.7 mm
Gap in Ring, d	0.2 mm

Table 2. Optimized dimensions of the SRR

Parameter	Dimensions
Length of Ring, a	3.7 mm
Inter-ring Spacing, b	0.2 mm
Width of Ring, c	0.5 mm
Gap in Ring, d	0.2 mm

5.1. Parameter Extraction of the Proposed Metamaterial Resonator

Determining the effective permittivity and permeability values of the resonator depicted in Figure 2 is accomplished using the NRW approach. Figures 3 and 4 show this, respectively. By altering the electromagnetic characteristics, the suggested unit cell produces a resonant frequency with negative permeability and permittivity.

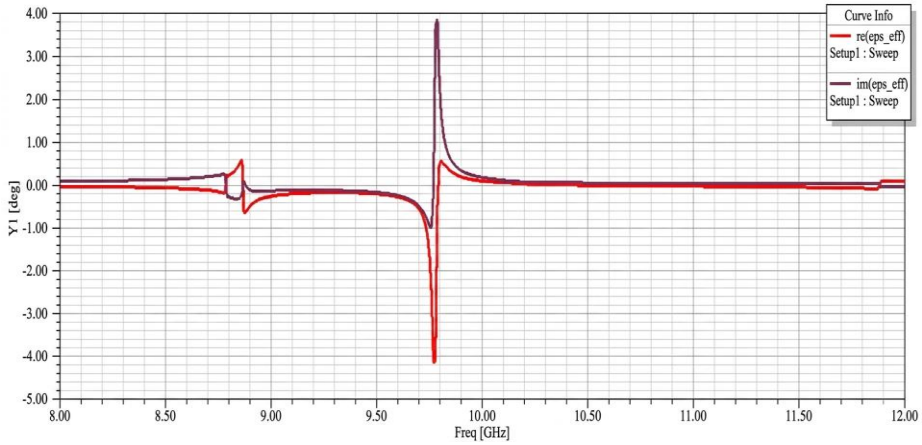

Fig. 3 Permittivity of the proposed resonator

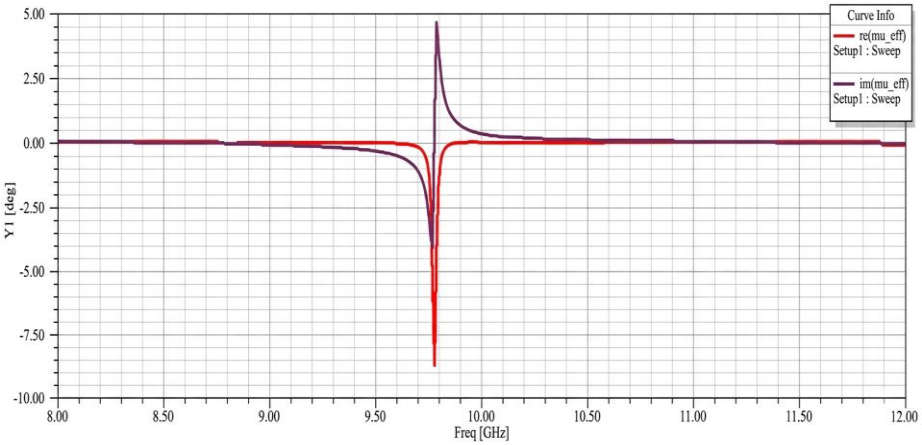

Fig. 4 Permeability of the proposed resonator

5.2. Parametric Examination of the Proposed Metamaterial Resonator

The proposed unit cell is subjected to a parametric study using ANSYS HFSS. The study examines the effect of varying ring width and ring gap measurements on capacitance and inductance at different frequencies. In Figure 5, we can see that there is a 200 MHz frequency increase with a bigger ring gap. A frequency increase of 150 MHz is the outcome of the ring width enlargement seen in Figure 6. Frequency is influenced by relative permittivity, as shown in Figure 7. Because a lower resonant frequency is caused by a higher relative permittivity, the resonator exhibits an enhanced effective capacitance.

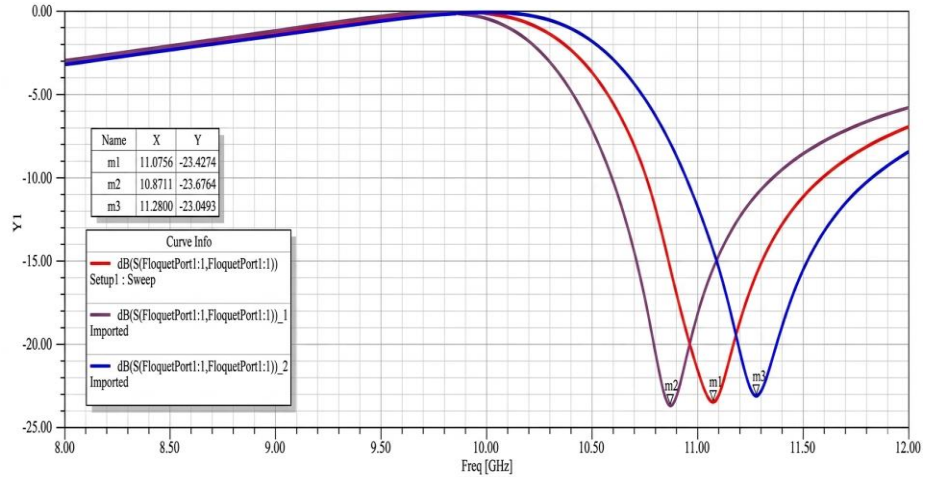

Fig. 5 Parametric analysis of the SRR for different ring gap

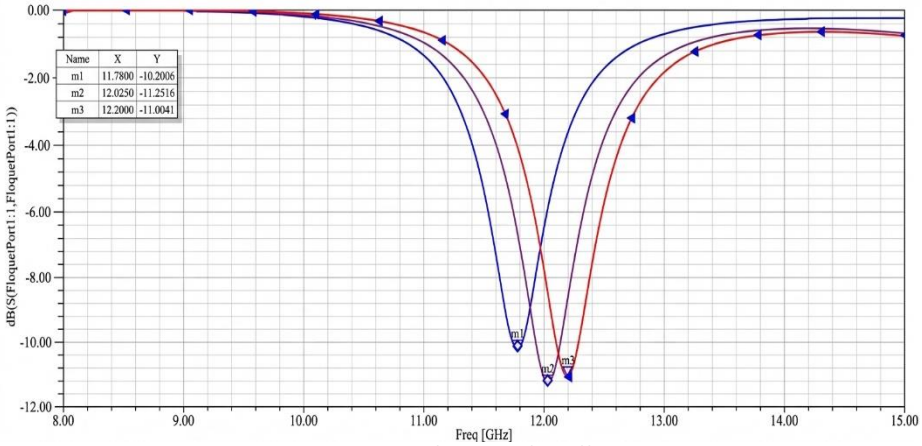

Fig. 6 Parametric analysis of the SRR for different ring width

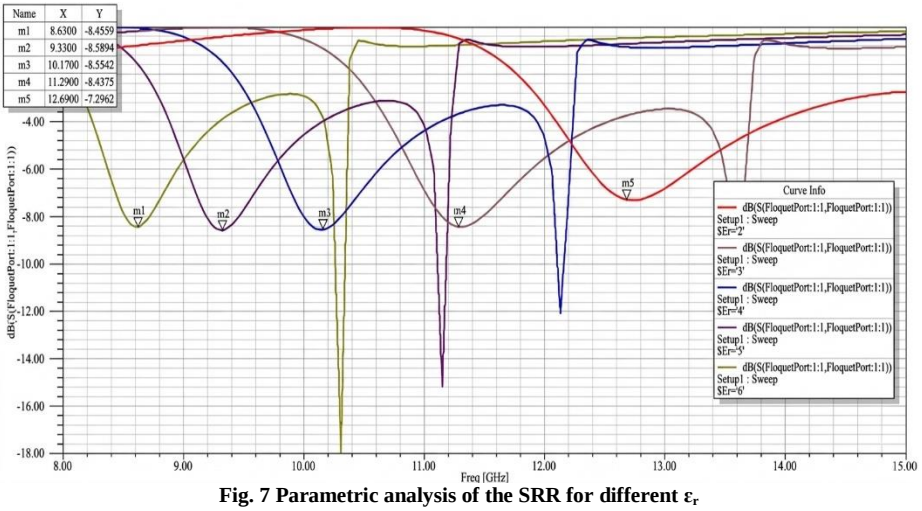

Fig. 7 Parametric analysis of the SRR for different ε_r

6. Open-Ended Coupled Line Filter

Figure 8 depicts a new planar BPF design that makes use of an open-ended linked line element. A substrate material with a relative permittivity of 3.55 and a thickness of 0.85 mm, RT/Duroid 4003, is utilized in the filter design. The filter is built from a number of important parts. Coupled microstrip lines enable the bandpass filter's primary resonating components to operate. Distance between lines, line width, and coupled section length are the three variables that determine coupling strength.

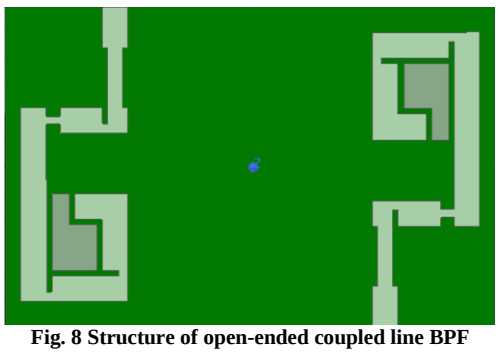

Fig. 8 Structure of open-ended coupled line BPF

Reduced gaps strengthen connections. A line's width defines its characteristic impedance, whereas its connected sections' length determines their resonant frequency. Line spacing in the microstrip resonator influences the filter's center frequency, bandwidth, and selectivity. The filter has parallel traces that are close together, demonstrating strong electromagnetic coupling. Electromagnetic coupling creates even-mode and odd-mode signals from transmission cables. Open-ended traces act as resonant stubs, improving filtering. These stubs increase transmission zeros and stopband attenuation. Open-ended portions introduce capacitance and shape the frequency response.

Two identical left and right resonators provide a balanced symmetrical filter with consistent frequency response and low insertion loss. The technique reduces production faults and balances results.

The filter inputs and outputs signal via feedlines. Energy flows between the first and last resonators via the lines. Insertion loss is controlled, and impedance matching is improved to prevent signal reflection.

6.1. Even and Odd Mode Analysis of the Open-Ended Coupled Line Filter

The paired transmission lines of the microstrip configuration enable electromagnetic coupling due to their proximity. The even and odd modes define potential propagation modes. The two modes yield distinct characteristic impedances, leading to varying effective permittivity values.

6.1.1. Even Mode

The currents in both lines demonstrate unidirectional flow. The equivalent capacitance of the system increases during even-mode excitation due to heightened electric field concentration in the dielectric material.

$$Z_e = \frac{Z_0}{\sqrt{1+k}} \tag{17}$$

6.1.2. Odd Mode

The currents on both lines are oriented in opposing directions. Under odd-mode excitation, the electromagnetic fields exhibit heightened concentration in the air area, resulting in varying effective permittivity values.

$$Z_o = \frac{Z_0}{\sqrt{1-k}} \tag{18}$$

Equations (19)-(20) describe the effective dielectric constant ϵeff for both even and odd modes.

$$\epsilon_{\text{eff,e}} = \frac{\epsilon_r+1}{2} + \frac{\epsilon_r-1}{2}\left(\frac{1}{\sqrt{1+12h/w}}\right) \tag{19}$$

$$\epsilon_{\text{eff,o}} = \frac{\epsilon_r+1}{2} + \frac{\epsilon_r-1}{2}\left(\frac{1}{\sqrt{1+12h/w+0.04(1-w/h)^2}}\right) \tag{20}$$

The relative permittivity of the substrate εr, the height of the substrate 'h', and the width of the microstrip lines 'w' are defined by Equations (19)-(20). The following are the resonance criteria for coupled resonators, which can accommodate modes of either even or odd order:

$$f_e = \frac{c}{2L_{\text{cff}}\sqrt{\epsilon_{\text{eff,e}}}} \tag{21}$$

$$f_o = \frac{c}{2L_{\text{cff}}\sqrt{\epsilon_{\text{eff,o}}}} \tag{22}$$

Where f_e signifies even-mode resonance frequency, and f_o denotes odd-mode resonance frequency. Leff is the effective length of the section, which is calculated as:

$$L_{\text{eff}} = \frac{c}{2f_0\sqrt{\epsilon_{\text{eff}}}} \tag{23}$$

Coupled-Line BPF, which runs at 9.7 GHz and is made of RT/Duroid 4003 material with a dielectric constant of 3.55, has its results for both even and odd mode testing presented in Table 3.

Table 3. Summary of even and odd mode analysis

Parameter	Value
Even-Mode Permittivity	2.73
Odd-Mode Permittivity	2.73
Even-Mode Impedance	47.67 Ω
Odd-Mode Impedance	52.70 Ω
Even-Mode Resonant Frequency	9.69 GHz
Odd-Mode Resonant Frequency	9.70 GHz

The filter's balanced performance is the outcome of the fact that it's even-mode and odd-mode permittivity exhibit identical values. The system is able to match impedances correctly because of its two modal impedances, which are about 50 Ω each.

6.2. Frequency Response of the Open-Ended Coupled Line Filter

Figure 9 displays the frequency response of the open-ended coupled line BPF. There are noticeable notches at 9.99 GHz and 10.86 GHz, where the graph shows a sudden change from passband to stopband.

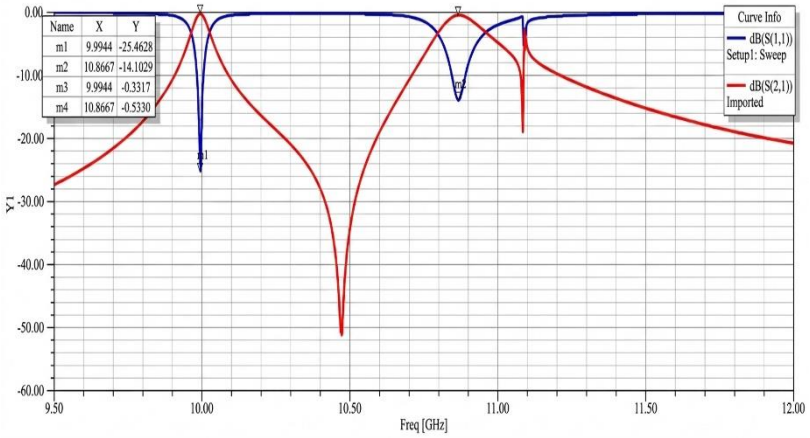

Fig. 9 Frequency response of Open-Ended coupled line BPF

At these frequencies, there are transmission zeros, which improve stopband attenuation and confirm effective selectivity. At 9.99 GHz, the attenuation is 25.46 dB. At 10.86 GHz, the rejection is 14.10 dB. There is a significant loss of undesired signals due to the response's deep notches. With an S12 measurement of 0.33 dB at 9.99 GHz, the system is said to have very little insertion loss. Since the majority of the signal power is able to flow through the filter, the system demonstrates negligible insertion loss. The system achieves complete impedance matching at 9.99 GHz, as S11 measures 25.46 dB. Designed for wideband applications, this filter boasts a bandwidth of 870 MHz.

6.3. Group Delay Analysis

The group delay of the proposed bandpass filter is related to the phase response of the transmission coefficient (S_{21}) and is defined as the negative derivative of the transmission phase with respect to angular frequency. Although the explicit group delay plot is not presented, the phase response shown in Figure 10 exhibits a smooth and nearly linear variation within the passband region, indicating stable group delay characteristics. It is observed that the phase variation does not exhibit abrupt nonlinearities within the passband, which suggests minimal signal distortion and good phase linearity. This behavior confirms that the proposed filter is suitable for high-frequency communication applications where signal integrity is critical.

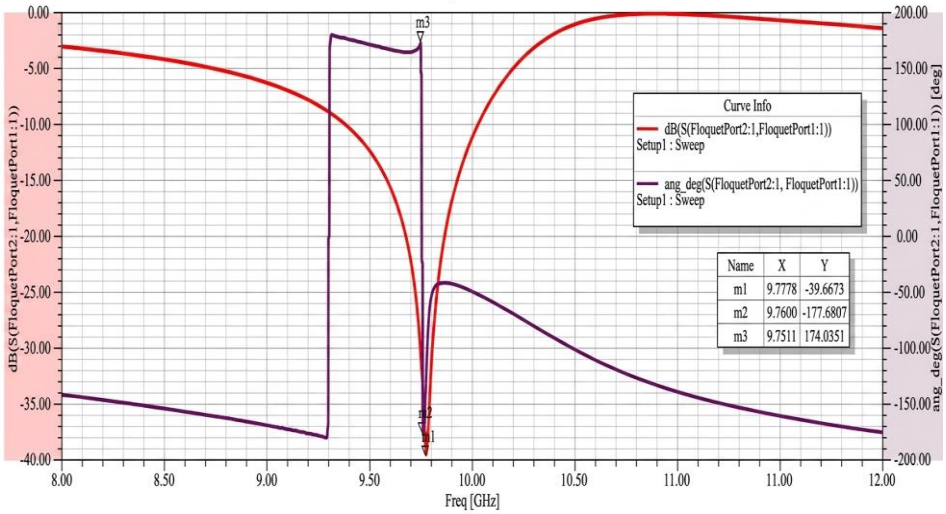

Fig. 10 Group delay

6.4. Integration of SRR in Open-Ended Coupled Line Filter

The designed BPF's geometrical characteristics are displayed in Table 4. Adding twin SRRs operating at 16.2 x 10.2 mm³ improves the open-ended coupled-line BPF system's efficiency (Figure 11).

For better near-field coupling, SRRs focus electromagnetic fields onto a small region. Additional paths for energy transfer among resonators are made possible by the capacitive gaps in the SRRs.

A decrease in radiation losses allows the system to have a better filter efficiency. Scientists manipulate the intensity of the coupling between coupled-line resonators and SRRs by adjusting the distance between the two.

Stronger coupling, caused by the close proximity of the SRRs, results in a broader bandwidth. Beyond the microstrip line connections, the SRRs provide additional capacitively and inductively coupled channels. Better field interactions, brought about by the extra pathways, alter the filter's signal transmission capabilities.

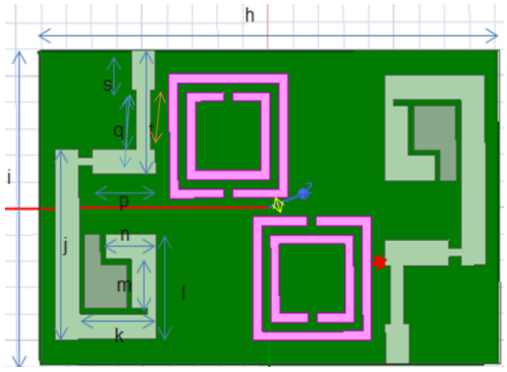

Fig. 11 Open-ended coupled line BPF incorporating twin SRRs

Table 4. Parameters of open-ended coupled Line BPF incorporating twin SRRs

Parameter	Value (mm)	Parameter	Value (mm)
h	16.2	n	2.0
i	10.2	p	2.5
j	7.2	t	4.6
k	2.4	q	2.8
l	4.0	s	1.5
m	1.8		

6.5. Frequency Response of Open-Ended Coupled Line Filter Integrating Twin SRRs

The filter's frequency response is seen in Figure 12. The differences in performance metrics between SRR-based and non-SRR-based tests are displayed in Table 5. By incorporating the twin SRRs into the open-ended coupled-line structure, the system's effective inductance and capacitance are altered, and new resonant routes are generated.

The end consequence is an increase in bandwidth due to the several closely spaced resonant modes. In addition, transmission zeros are formed around the passband margins as a result of the interaction between the SRRs and the transmission line. These transmission zeros increase the filter's selectivity by creating a sharp drop-off and better out-of-band rejection. As a result, the twin SRR setup boosts filtering performance and frequency responsiveness while simultaneously increasing bandwidth.

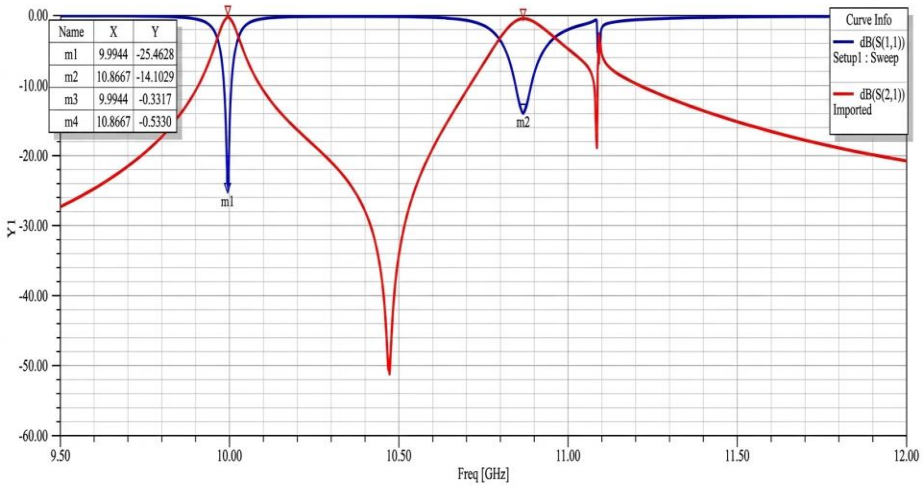

Fig. 12 Frequency response of open-ended coupled line BPF

Table 5. Comparison of performance parameters with and without SRRs

Parameter	Without SRR	With SRR
Out-of-Band Frequency Rejection	25.46 dB, 14.10 dB	37.91 dB, 21.08 dB
Insertion Loss	0.33 dB	0.34 dB
Reflection Loss	25.46	24.94
Bandwidth	870 MHz	1.26 GHz

6.6. Validation and Practical Considerations

The proposed metamaterial-inspired BPF has been validated using full-wave electromagnetic simulations, which are widely accepted for the design and analysis of microwave and RF components. The simulation results presented in this work are obtained using a high-frequency electromagnetic solver, ensuring accurate modeling of distributed effects, coupling mechanisms, and material properties.

To ensure the robustness and reliability of the proposed design, multiple levels of validation have been incorporated. First, a detailed parametric analysis of the SRR has been performed, examining the influence of ring gap, ring width, inter-ring Spacing, and substrate permittivity on the resonance characteristics. This analysis demonstrates that the resonator behavior follows the expected LC resonance model, thereby validating the theoretical foundation of the design.Second, the open-ended coupled-line filter has been analyzed using even- and odd-mode theory. The calculated modal impedances and effective permittivity values are in close agreement with the simulated results, confirming the correctness of the design methodology and the resonance conditions. The close proximity of even- and odd-mode resonant frequencies further indicates balanced coupling and proper impedance matching.

Third, the effect of twin SRR integration has been systematically evaluated by comparing the filter performance with and without SRR loading. The results clearly demonstrate that the inclusion of SRRs enhances electromagnetic coupling, improves field confinement, and introduces additional transmission zeros, leading to improved selectivity and out-of-band rejection. The observed improvement in bandwidth (from 870 MHz to 1.26 GHz) and rejection characteristics provides strong evidence of the effectiveness of the proposed approach. In addition, the obtained performance metrics have been compared with reported results in the literature. The proposed design achieves a favorable combination of low insertion loss, wider bandwidth, compact size, and enhanced rejection, which further validates its effectiveness relative to existing filter designs. Although experimental validation is not included in the present work, the simulation-based results are supported by well-established theoretical models and comparative analysis. In practical implementations, certain deviations may arise due to fabrication tolerances, conductor losses, dielectric constant variations, and connector mismatches. These effects may lead to slight shifts in resonant frequency and minor

degradation in insertion loss or return loss. However, the overall filter behavior and performance trends are expected to remain consistent with the simulated results. The proposed structure is compatible with standard Printed Circuit Board (PCB) fabrication techniques and can be implemented using commercially available microwave substrates. Therefore, the design is practically realizable, and experimental validation will be carried out in future work to further confirm the simulated performance.

6.7. Comparative Evaluation with the Recent Work

The comparison spans multiple filter technologies to provide a comprehensive evaluation of the proposed design, as illustrated in Tables 6 and 7. Cavity resonator-based filters demonstrate very low insertion loss and high-quality factor; however, they suffer from bulky three-dimensional structures and are not suitable for compact planar integration in modern RADAR front-end systems. Similarly, SAW and BAW filters offer compact chip-scale implementations with good frequency stability, but they are generally limited to lower frequency bands and exhibit relatively narrow fractional bandwidth. Moreover, their fabrication requires specialized materials and processes, making them less compatible with conventional microwave PCB technologies. Plasmonic and SSPP-based filters provide wider fractional bandwidth and strong electromagnetic field confinement. However, these designs often exhibit limited out-of-band rejection and involve complex geometrical structures, which can increase fabrication difficulty and reduce design flexibility for practical applications.

Recent meta material-based filters demonstrate ultra-wideband performance; however, they are typically designed for broadband applications rather than targeted X-band operation. As a result, they lack the frequency selectivity and controlled passband characteristics required for RADAR and satellite communication systems. In contrast, conventional SRR/CSRR-based planar filters reported generally achieve compact size but suffer from higher insertion loss, narrow bandwidth, or insufficient control over out-of-band rejection due to weak resonator coupling. The proposed twin SRR-loaded open-ended coupled-line bandpass filter addresses these limitations by providing a balanced combination of performance parameters specifically tailored for X-band operation. The design achieves a center frequency of 9.7 GHz with a low insertion loss of 0.34 dB, a fractional bandwidth of approximately 13%, and a significantly enhanced out-of-band rejection of up to 37.91 dB. Additionally, the compact planar size of 16 × 10 mm² makes the proposed filter suitable for integration in practical microwave front-end systems. The improved performance is primarily attributed to the strong electromagnetic coupling introduced by the twin SRR configuration, which enhances field confinement and enables the generation of transmission zeros near the passband edges. This results in sharper selectivity and improved stopband suppression compared to existing designs. Overall, compared to both conventional and recent filter technologies, the proposed design offers a superior trade-off between bandwidth, insertion loss, selectivity, and compactness, making it a highly suitable candidate for X-band RADAR and satellite communication applications.

Table 6. Comparative analysis of conventional filter technologies and superiority of proposed SRR-Based X-Band bandpass filter

Technology	Key Limitations	Impact on Performance	How Proposed SRR-Based Design Overcomes
Lumped Element Filters	• Strong parasitic effects at high frequency • Low self-resonant frequency of L and C • Poor bandwidth control • High insertion loss • Large PCB footprint	•Unstable response at X-band •Increased loss and reduced efficiency •Limited bandwidth capability	• Uses distributed microstrip and SRR • Eliminates parasitic dominance • Achieves wide bandwidth (1.26 GHz) • Low insertion loss (0.34 dB)
Cavity Resonator Filters	• Very large size and weight • Complex machining • Difficult integration with planar circuits • Narrowband operation	• Not suitable for compact RF front ends • High cost and poor scalability	• Planar microstrip structure (compact: 16×10 mm²) • Easy PCB fabrication • Suitable for integrated RF modules • Wideband performance
SAW / BAW Filters	• Limited bandwidth capability • Lithographic limitations at high frequency • Reduced efficiency at higher GHz range • Limited power handling	• Not suitable for wideband X-band systems • Performance degradation at high frequency	• Electromagnetic resonance-based design • No lithographic constraints • Supports wideband and high-frequency operation
Plasmonic Filters (SIPW/SSPP)	• High propagation loss • Complex structures • Difficult PCB integration	• Increased insertion loss • Limited practical implementation	• Simple planar geometry • Reduced loss due to localized SRR coupling

	• High fabrication cost		• Compatible with standard PCB fabrication
Conventional Planar Resonator Filters	• Narrow bandwidth • High conductor/dielectric loss • Poor harmonic suppression • Requires additional structures for selectivity	• Limited selectivity and bandwidth • Increased design complexity	• Twin SRR introduces additional transmission zeros • Enhanced selectivity and sharp roll-off • Improved bandwidth and rejection
Existing SRR-Based Filters	• Weak coupling • Narrow fractional bandwidth • Higher insertion loss in cascaded designs • Limited tuning capability	• Limited performance improvement • Not optimized for X-band wideband applications	• Twin SRR configuration enhances coupling • Bandwidth improved (870 MHz → 1.26 GHz) • Strong out-of-band rejection (37.91 dB) • Compact and optimized design

Table 7. Comparative evaluation with existing literature

Ref.	f_0 (GHz)	Technology	Material	IL (dB)	RL (dB)	FBW	Size
[8]	20.0	Cavity Resonators		0.3	17	1%	110x22x20 mm^3
[13]	14.2	Cavity Resonators		0.5	17	1%	18x18x12 mm^3
[16]	3.5	SAW/BAW	AlN	3.0	18	5%	3x5 mm^2
[21]	10.2	SIPW	Roger 5880	1.5	10	40%	36x18 mm^2
[22]	8.7	SIPW	FR-4	2.0	10	32%	34x12 mm^2
[25]	1.0	Planar	Roger 4003	2.5	15	1%	30x20 mm^2
[29]	2.4	SRR/CSRR	Roger 6010	2.5	16	5%	25x19 mm^2
[30]	1.0	SRR/CSRR	FR-4	1.5	16	20%	30x18 mm^2
[31]	9.0	SRR/CSRR	Roger 5880	3.8	15	1%	25x22 mm^2
[3]	5.0, 8.9	SRR/CSRR	Roger 4003	6.2, 5.2	12, 18	6%, 3%	20x24 mm^2
[32]	2.4	SRR/CSRR	Roger 6010	1.3	19	5%	26x26 mm^2
[34]	3.6	SRR/CSRR	Roger 5880	1.9	16	5%	27x18 mm^2
[1]	6.5	Metamaterial	Roger 5880	2.1	12	20%	30x22 mm^2
[40]	4.0	SRR	Roger 5880	3.0	12	10%	20x15 mm^2
[41]	6.5	SIW+CSRR	FR-4	3.3	15	40%	20x30 mm^2
[42]	4.8	HMSIW + CSRR + DGS	Roger 5880	2.5	15	9%	30×17 mm^2
[43]	6.0	Metamaterial	FR-4	3.0	18	8%	30x20 mm^2
Present Work	9.7	SRR	Roger 4003	0.3	24	13%	16x10 mm^2

7. Conclusion and Future Scope

This research created an open-ended coupled-line bandpass filter which uses a metamaterial design and two SRRs for operation in X-band RADAR and satellite communication applications. The researchers conducted a complete structural investigation of the SRR, which established direct connections between the Ring's geometric design and its resonant characteristics. The research used the NRW method to obtain effective material parameters, which showed that the material exhibited negative permittivity and magnetic resonance at the operational frequency, thus proving the resonator's metamaterial characteristics.

The design process for the open-ended coupled-line filter required the application of even- and odd-mode analysis to create proper operational balance and achieve precise impedance matching. The twin SRRs were positioned within the coupled-line region to create a strong coupling effect, which enabled the system to gain two extra pathways for inductive and capacitive interactions. The proposed filter achieved a bandwidth increase from 870 MHz to 1.26 GHz while the system maintained an extremely low insertion loss of 0.34 dB. The out-of-band rejection increased to 37.91 dB, which indicates the system achieved high selectivity and better capability to eliminate undesired signals. The roll-off characteristics received enhancement through the appearance of transmission zeros close to the passband boundaries.

The proposed SRR-loaded BPF provides better performance than any previous filter designs, according to comparative testing results, which evaluate its bandwidth selectivity, insertion loss, and compactness attributes. The

filter brings multiple advantages that make it suitable for use in X-band RADAR front ends and satellite transceivers, and broadband microwave communication systems, which require both wide bandwidth and effective interference rejection capabilities.

Researchers will investigate advanced metamaterial-assisted filter designs that build upon the existing filter architecture. The ground plane should be designed to use CSRRs or hybrid SRR-CSRR configurations because they will create extra transmission zeros while maintaining circuit simplicity and enhancing stopband suppression. Researchers can use multi-resonator SRR arrays that have spatial periodicity control to study how they affect dispersion patterns and create better selectivity through sharper skirt control. The open-ended coupled-line topology enables users to create multiple wireless communication bands and extensive frequency ranges through strategic SRR configurations, which operate at different electrical lengths to create multiple resonance points. The approach provides compact filtering solutions that enable separate passbands for multi-channel RADAR and satellite payload operations.

References

[1] Mouhssine Elbathaoui et al., "A Compact UWB Bandpass Filter based on Metamaterials for Sub-6 GHz 5 G and cmWave Band 6 G Wireless Communications," *Franklin Open*, vol. 13, pp. 1-12, 2025. [CrossRef] [Google Scholar] [Publisher Link]

[2] Ampavathina Sowjanya, and Damera Vakula, "Metamaterial-Inspired Compact Single and Multiband Filters," *Advances in Science, Technology and Engineering Systems Journal*, vol. 7, no. 4, pp. 92-97, 2022. [CrossRef] [Google Scholar] [Publisher Link]

[3] Mohammed Berka et al., "Dual-Band Bandpass Filter based on Electromagnetic Coupling of Twin Square Metamaterial Resonators (SRRs) and Complementary Resonator (CSRR) for Wireless Communications," *Journal of Electronic Materials*, vol. 50, no. 8, pp. 4887-4895, 2021. [CrossRef] [Google Scholar] [Publisher Link]

[4] Monica Martinez-Mendoza et al., "Design of a Triband Lumped Element Filter for Digital Microwave Power Amplifiers," *2015 European Microwave Conference (EuMC)*, Paris, France, pp. 805-808, 2015. [CrossRef] [Google Scholar] [Publisher Link]

[5] Matthew A. Morgan, and Tod A. Boyd, "Theoretical and Experimental Study of a New Class of Reflectionless Filter," *IEEE Transactions on Microwave Theory and Techniques*, vol. 59, no. 5, pp. 1214-1221, 2011. [CrossRef] [Google Scholar] [Publisher Link]

[6] Muhammad Ali et al., "Miniaturized High-Performance Filters for 5G Small-Cell Applications," *2018 IEEE 68th Electronic Components and Technology Conference (ECTC)*, Diego, CA, USA, pp. 1068-1075, 2018. [CrossRef] [Google Scholar] [Publisher Link]

[7] Muhammad Ali et al., "First Demonstration of Compact, Ultra-Thin Low-Pass and Bandpass Filters for 5G Small-Cell Applications," *IEEE Microwave and Wireless Components Letters*, vol. 28, no. 12, pp. 1110-1112, 2018. [CrossRef] [Google Scholar] [Publisher Link]

[8] Bahram Yassini, Ming Yu, and Brian Keats, "A *Ka*-Band Fully Tunable Cavity Filter," *IEEE Transactions on Microwave Theory and Techniques*, vol. 60, no. 12, pp. 4002-4012, 2012. [CrossRef] [Google Scholar] [Publisher Link]

[9] Bahram Yassini, and Ming Yu, "A Novel Ka Band Dual Mode Super Q Cavity Filter," *IEEE MTT-S International Microwave Symposium (IMS2014)*, FL, USA, pp. 1-3, 2014. [CrossRef] [Google Scholar] [Publisher Link]

[10] Bahram Yassini, and Ming Yu, "Ka-Band Dual-Mode Super Q Filters and Multiplexers," *IEEE Transactions on Microwave Theory and Techniques*, vol. 63, no. 10, pp. 3391-3397, 2015. [CrossRef] [Google Scholar] [Publisher Link]

[11] Hai Hu, Ke-Li Wu, and Richard J. Cameron, "Stepped Circular Waveguide Dual-Mode Filters for Broadband Contiguous Multiplexers," *IEEE Transactions on Microwave Theory and Techniques*, vol. 61, no. 1, pp. 139-145, 2013. [CrossRef] [Google Scholar] [Publisher Link]

[12] Trong-Hieu Le et al., "A Novel Diplexer Integrated with a Shielding Case using High *Q*-Factor Hybrid Resonator Bandpass Filters," *IEEE Microwave and Wireless Components Letters*, vol. 28, no. 3, pp. 215-217, 2018. [CrossRef] [Google Scholar] [Publisher Link]

[13] Michal Baranowski et al., "The Design of Cavity Resonators and Microwave Filters Applying Shape Deformation Techniques," *IEEE Transactions on Microwave Theory and Techniques*, vol. 71, no. 7, pp. 3065-3074, 2023. [CrossRef] [Google Scholar] [Publisher Link]

[14] Hualei wang et al., "Design of Ladder-Type SAW/BAW Filters with Constant Group Delay," *IEEE International Ultrasonics Symposium*, Orlando, FL, USA, pp. 345-348, 2011. [CrossRef] [Google Scholar] [Publisher Link]

[15] Dimitra Psychogiou, Roberto Gómez-García, and Dimitrios Peroulis, "SAW-based Bandpass Filters with Flat in-band Group Delay and Enhanced Fractional Bandwidth," *2017 IEEE MTT-S International Microwave Workshop Series on Advanced Materials and Processes for RF and THz Applications (IMWS-AMP)*, Pavia, Italy, pp. 1-3, 2018. [CrossRef] [Google Scholar] [Publisher Link]

[16] Xian-Hu Zha et al., "Surface and Bulk Acoustic Wave Resonators Based on Aluminum Nitride for Bandpass Filters," *AAPPS Bulletin*, vol. 34, no. 1, pp. 1-15, 2024. [CrossRef] [Google Scholar] [Publisher Link]

[17] Pu Chen, Guangxi Li, and Zhiyuan Zhu, "Development and Application of SAW Filter," *Micromachines*, vol. 13, no. 5, pp. 1-15, 2022. [CrossRef] [Google Scholar] [Publisher Link]

[18] Yasir I.A. Al-Yasir et al., "Recent Progress in the Design of 4G/5G Reconfigurable Filters," *Electronics*, vol. 8, no. 1, pp. 1-17, 2019. [CrossRef] [Google Scholar] [Publisher Link]

[19] Kai Yang et al., "Advanced RF Filters for Wireless Communications," *Chip*, vol. 2, no. 4, pp. 1-26, 2023. [CrossRef] [Google Scholar] [Publisher Link]

[20] Gabriel Giribaldi et al., "Compact and Wideband Nanoacoustic Pass-band Filters for Future 5G and 6G Cellular Radios," *Nature Communications*, vol. 15, no. 1, pp. 1-13, 2024. [CrossRef] [Google Scholar] [Publisher Link]

[21] Longfang Ye et al., "Substrate Integrated Plasmonic Waveguide for Microwave Bandpass Filter Applications," *IEEE Access*, vol. 7, pp. 75957-75964, 2019. [CrossRef] [Google Scholar] [Publisher Link]

[22] Yuxuan Luo et al., "A Compact Microwave Bandpass Filter based on Spoof Surface Plasmon Polariton and Substrate Integrated Plasmonic Waveguide Structures," *Applied Physics A*, vol. 128, no. 2, 2022. [CrossRef] [Google Scholar] [Publisher Link]

[23] Gaurav Mittal, and Nagendra Prasad Pathak, "Spoof Surface Plasmon Polaritons based Microwave Bandpass Filter," *Microwave and Optical Technology Letters*, vol. 63, no. 1, pp. 51-57, 2021. [CrossRef] [Google Scholar] [Publisher Link]

[24] Asad Aziz, "A Novel Plasmonic Waveguide for Extraordinary Field Enhancement of Spoof Surface Plasmon Polaritons with Low-Loss Feature," *Results in Optics*, vol. 5, pp. 1-9, 2021. [CrossRef] [Google Scholar] [Publisher Link]

[25] Chih-Jung Chen, "Design of Parallel-Coupled Dual-Mode Resonator Bandpass Filters," *IEEE Transactions on Components, Packaging and Manufacturing Technology*, vol. 6, no. 10, pp. 1542-1548, 2016. [CrossRef] [Google Scholar] [Publisher Link]

[26] Faroq Razzaz, Saud M. Saeed, and Majeed A.S. Alkanhal, "Ultra-Wideband Bandpass Filters using Tapered Resonators," *Applied Sciences*, vol. 12, no. 7, pp. 1-12, 2022. [CrossRef] [Google Scholar] [Publisher Link]

[27] Li Yang et al., "Novel Multilayered Ultra-Broadband Bandpass Filters on High-Impedance Slotline Resonators," *IEEE Transactions on Microwave Theory and Techniques*, vol. 67, no. 1, pp. 129-139, 2019. [CrossRef] [Google Scholar] [Publisher Link]

[28] A. Salim et al., "A Polygonal Open-Loop Resonator Compact Bandpass Filter for Bluetooth and WLAN Applications," *IOP Conference Series: Materials Science and Engineering*, vol. 433, no. 1, pp. 1-10, 2018. [CrossRef] [Google Scholar] [Publisher Link]

[29] Mohamad Syahral, and Achmad Munir, "Development of Multiple Elements of SRR-based Bandpass Filter," *2016 10th International Conference on Telecommunication Systems Services and Applications, TSSA*, Denpasar, Indonesia, pp. 1-4, 2017. [CrossRef] [Google Scholar] [Publisher Link]

[30] Zaid A. Abdul Hassain, Amer Abbood AL-Behadili, and Adham R. Azeez, "First Order Parallel Coupled BPF with Wideband Rejection based on SRR and CSRR," *Telkomnika Telecommunication Computing Electronics and Control*, vol. 17, no. 6, pp. 2704-2712, 2019. [CrossRef] [Google Scholar] [Publisher Link]

[31] Ria Lovina Defitri, and Achmad Munir, "X-band Microstrip Narrowband BPF Composed of Split Ring Resonator," *2016 Progress in Electromagnetics Research Symposium (PIERS)*, Shanghai, China, pp. 3468-3471, 2016. [CrossRef] [Google Scholar] [Publisher Link]

[32] Zenal Aripin et al., "Compact SRR-based Microstrip BPF for Wireless Communication," *2015 2nd International Conference on Information Technology, Computer, and Electrical Engineering (ICITACEE)*, Semarang, Indonesia, pp. 474-477, 2016. [CrossRef] [Google Scholar] [Publisher Link]

[33] Mohamed Hesham, and Sameh O. Abdellatif, "Compact Bandpass Filter based on Split Ring Resonators," *2019 International Conference on Innovative Trends in Computer Engineering (ITCE)*, Aswan, Egypt, pp. 301-303, 2019. [CrossRef] [Google Scholar] [Publisher Link]

[34] Chi-Hyung Ahn, Dong-Jin Jung, and Kai Chang, "Compact Parallel-Coupled Line Bandpass Filter using Double Complementary Split Ring Resonators," *Microwave and Optical Technology Letters*, vol. 55, no. 3, pp. 506-509, 2013. [CrossRef] [Google Scholar] [Publisher Link]

[35] Monish Gupta, and Jyoti Saxena, "Microstrip Filter Designing by SRR Metamaterial," *Wireless Personal Communications*, vol. 71, no. 4, pp. 3011-3022, 2013. [CrossRef] [Google Scholar] [Publisher Link]

[36] K.V. Vineetha, M. Siva Kumar, and B.T.P. Madhav, "Analysis of Triple Band Split Ring Resonator based Microstrip Bandpass Filter," *Journal of Physics: Conference Series*, vol. 1804, no. 1, pp. 1-7, 2021. [CrossRef] [Google Scholar] [Publisher Link]

[37] Jonathan Carver, Vianney Reignault, and Frédérique Gadot, "Engineering of the Metamaterial-based Cut-Band Filter," *Applied Physics A*, vol. 117, no. 2, pp. 513-516, 2014. [CrossRef] [Google Scholar] [Publisher Link]

[38] Seif Naoui, Latrach Latrach, and A. Gharsallah, "Equivalent Circuit Model of Double Split Ring Resonators," *International Journal of Microwave and Optical Technology*, vol. 11, no. 1, pp. 1-6, 2016. [Google Scholar]

[39] Edward J. Rothwell et al., "Analysis of the Nicolson-Ross-Weir Method for Characterizing the Electromagnetic Properties of Engineered Materials," *Progress in Electromagnetics Research*, vol. 157, pp. 31-47, 2016. [CrossRef] [Google Scholar] [Publisher Link]

[40] K. Naganarasaiah Goud et al., "Implementation of Band Pass Filter for Satellite Communications using CSRR Technique," *Proceedings of the 6th International Conference on Communications and Cyber Physical Engineering ICCCE*, Hyderabad, India, vol. 1096, pp. 417-425, 2024. [CrossRef] [Google Scholar] [Publisher Link]

[41] Senathipathi Udhayanan, and Krishnan Shambavi, "Metamaterial-based Compact UWB Bandpass Filter using Substrate Integrated Waveguide," *Progress in Electromagnetics Research Letters*, vol. 120, pp. 1-6, 2024. [CrossRef] [Google Scholar] [Publisher Link]

[42] Soundarya Gopalakrishnan et al., "DMS, CSRR, and DGS Loaded HMSIW Dual-Band Filter with Closely Set Apart Passbands," *Progress in Electromagnetics Research C*, vol. 146, pp. 187-193, 2024. [CrossRef] [Google Scholar] [Publisher Link]

[43] Khyati Chavda, and A.K. Sarvaiya, "Design, Simulate and Compare Band Stop Filter of Different Hexagonal Metamaterial Shapes Resonators," *International Journal of Microwave and Optical Technology*, vol. 17, no. 5, 2022. [Google Scholar] [Publisher Link]